

Force, charge, and conductance of an ideal metallic nanowire

F. Kassubek

Fakultät für Physik, Albert-Ludwigs-Universität, Hermann–Herder–Str. 3, D-79104 Freiburg, Germany

C. A. Stafford

Fakultät für Physik, Albert-Ludwigs-Universität, Hermann–Herder–Str. 3, D-79104 Freiburg, Germany
and

*Physics Department, University of Arizona, Tucson, AZ 85721**

Hermann Grabert

Fakultät für Physik, Albert-Ludwigs-Universität, Hermann–Herder–Str. 3, D-79104 Freiburg, Germany
(November 22, 2017)

The conducting and mechanical properties of a metallic nanowire formed at the junction between two macroscopic metallic electrodes are investigated. Both two- and three-dimensional wires with a W(ide)–N(arrow)–W(ide) geometry are modelled in the free-electron approximation with hard-wall boundary conditions. Tunneling and quantum-size effects are treated exactly using the scattering matrix formalism. Oscillations of order E_F/λ_F in the tensile force are found when the wire is stretched to the breaking point, which are synchronized with quantized jumps in the conductance. The force and conductance are shown to be essentially independent of the width of the wide sections (electrodes). The exact results are compared with an adiabatic approximation; the later is found to overestimate the effects of tunneling, but still gives qualitatively reasonable results for nanowires of length $L \gg \lambda_F$, even for this abrupt geometry. In addition to the force and conductance, the net charge of the nanowire is calculated and the effects of screening are included within linear response theory. Mesoscopic charge fluctuations of order e are predicted which are strongly correlated with the mesoscopic force fluctuations. The local density of states at the Fermi energy exhibits nontrivial behavior which is correlated with fine structure in the force and conductance, showing the importance of treating the whole wire as a mesoscopic system rather than treating only the narrow part.

PACS numbers: 73.23.Ps, 62.20.Fe, 73.40.Jn

I. INTRODUCTION

Metallic nanowires may be formed at the junction between two metallic electrodes which are pressed together and/or pulled apart in a controlled fashion.^{1–6} In a wire of nanoscopic cross section, the transverse motion is quantized, leading to a finite number of electronic modes below the Fermi energy E_F which can be transmitted through the wire. A striking consequence of these discrete modes is the quantization of the wire's conductance at integer multiples of $G_0 = 2e^2/h$, a phenomenon first observed in two-dimensional (2D) semiconductor heterostructures,^{7–9} and subsequently studied in detail in three-dimensional (3D) metallic nanowires.^{1–3,6} A subtlety inherent in conductance quantization experiments is that even for a nearly ideal nanowire, the presence of disorder in the electrodes far from the region of interest leads to a suppression of the conductance plateaus below integer values. This suppression is normally taken into account by subtracting a phenomenological series resistance,^{3,6–8} which allows one to shift the experimentally observed plateaus back to integer values. Theoretical histograms^{10–12} exhibit a similar shift towards lower values of the conductance, though the precise form of the suppression is not equivalent to a simple series resistance due to quantum interference effects.^{13,14} These considerations underline the importance of treating the nanowire and the electrodes connected to it as a single mesoscopic system, rather than considering the nanowire in isolation.

The cohesive properties of good metals are also determined to a large extent by the conduction electrons. Thus, one may expect the mode quantization in a nanowire to have a strong effect on its mechanical properties as well.¹⁵ In a pioneering experiment published in 1996, Rubio, Agraït, and Vieira measured simultaneously the force and conductance during the formation and rupture of an atomic-scale Au nanowire.⁴ They observed oscillations in the tensile force of order lnN under deformation, which were synchronized with jumps of order $2e^2/h$ in the conductance. Similar experimental results were obtained independently by Stalder and Dürig.⁵ In a previous paper,¹⁵ it was shown that this intriguing behavior can be understood quantitatively using a simple free-electron jellium model for a metallic nanowire. The theoretical approach introduced by Stafford, Baeriswyl, and Bürki¹⁵ uses the electronic scattering matrix to describe the coupling of the nanowire of interest to the macroscopic probes (*e.g.*, STM/AFM) used to manipulate it; the correct treatment of this coupling is crucial for calculating the mesoscopic corrections to the bulk

electrical and mechanical properties. In the previous paper, the scattering matrix was evaluated using the adiabatic and WKB approximations, appropriate for a smooth geometry in which the diameter D of the nanowire varies slowly along its symmetry axis z , *i.e.*, $(dD/dz)^2 \ll 1$. The qualitative picture which emerged from the analysis of Ref. 15 is that each quantized mode contributing $2e^2/h$ to the conductance of the nanowire also contributes an amount of order E_F/λ_F to its cohesive force, where λ_F is the De Broglie wavelength of electrons at the Fermi energy E_F . (For monovalent metals, E_F/λ_F is of order 1nN.) Under elongation, the cross section of the nanowire narrows, and each time a transverse mode is cut off, both the conductance and the cohesive force decrease abruptly. Using an elegant argument based on the technique of Ref. 15, H\"opppler and Zwerger showed that the leading order mesoscopic correction to the tensile force depends only on the topology of the cross section of the nanowire.¹⁶ The scattering matrix formalism has also been used to study the effects of impurity scattering on the mechanical properties of nanowires.¹⁷

Independently, van Ruitenbeek, Devoret, Esteve, and Urbina¹⁸ considered wires with a special W(ide)–N(arrow)–W(ide) geometry, with two wide outer sections, representing the electrodes, and a narrow inner section of constant diameter, representing the nanowire (see Fig. 1). They considered the limit (cf. also Refs. 19,20) where the narrow section is sufficiently long that the boundary effects at the junctions of the wide and narrow sections give a negligible contribution to the energetics of the nanowire. They also pointed out that screening should be included, and imposed a charge neutrality constraint as a first approximation. However, they noted that the assumption of local charge neutrality of the nanowire breaks down for very short wires, such as those investigated in the experiments of Refs. 2–6, which are only of order 1nm in length. For such short wires, boundary effects are important.

In the present article, we investigate both 2D and 3D wires with the WNW geometry, treating the boundary effects arising from the connection of the nanowire to the electrodes exactly via the scattering matrix approach. Our results for the force in the WNW geometry are qualitatively similar to the results for smooth geometries presented in Ref. 15, although the presence of sharp corners is shown to lead to a non-generic topological correction to the force for small deformations from an ideal wire, which is well understood. The exact results for the WNW geometry are compared with an adiabatic approximation, which is found to overestimate the effects of tunneling, but still gives qualitatively reasonable results for the conductance and force of nanowires of length $L \gg \lambda_F$, even for this abrupt geometry. The local density of states at the Fermi energy is also calculated, and is shown to exhibit strong modulation on a length scale of order λ_F . This electronic structure of the scattering states gives vivid pictorial support of the notion¹⁵ that conductance channels act as metallic bonds.

In addition to the force and conductance, the net charge of the nanowire is calculated, and the effects of screening are addressed by a linear response approach. We predict mesoscopic charge fluctuations of order the fundamental charge quantum e , which are synchronized with the quantized steps in the wire's conductance, and strongly correlated with the mesoscopic force fluctuations. Similar charge fluctuations are predicted in 2D and 3D nanowires; they should thus be present in quasi-two-dimensional quantum point contacts exhibiting conductance quantization^{7–9} as well. The smallness of the predicted mesoscopic charge imbalance leads us to neglect electron-electron interactions in our treatment of the conducting and mechanical properties of the nanowire. Indeed, we find that the mesoscopic corrections to the force for wires of length $L \sim \lambda_F$ are large compared to the corrections expected due to screening effects, justifying our approach.

The paper is organized as follows: In Sec. II, we review the scattering matrix formulation of electrical conduction and statistical mechanics. General expressions for the force, charge and conductance of a mesoscopic conductor in terms of the electronic scattering matrix are derived. In Sec. III, the scattering matrix for 2D and 3D wires with the WNW geometry is calculated. For simplicity, 3D wires with a square cross section are considered, but it is straightforward to use our method for wires of arbitrary cross section if the eigenfunctions and eigenvalues of the 2D Schrödinger equation with Dirichlet boundary conditions for this shape are known. In Sec. IV, the results for the force, charge, and conductance of a 2D nanowire are presented. The semiclassical approximation to the force and charge, and the topological contribution due to sharp corners are discussed. The exact results are compared to an adiabatic approximation, and the local density of states at the Fermi energy is calculated. In Sec. V, the results for the force, charge, and conductance of 3D nanowires are presented. The effects of screening are evaluated within linear response. The relevance of our results to the experiments of Refs. 4 and 5 is discussed. Some general conclusions are presented in Sec. VI, and a comparison of the jellium model used here to atomistic descriptions of nanowires based on classical molecular dynamics simulations^{21–23} is given.

II. S-MATRIX FORMALISM

A nanowire connecting two macroscopic electrodes (depicted schematically in Fig. 1) is an open quantum mechanical system. The Schrödinger equation for such an open system is most naturally formulated as a scattering problem.

The fundamental quantity describing the properties of the system is the scattering matrix $S(E)$ connecting incoming and outgoing asymptotic states of conduction electrons in the electrodes. (The degrees of freedom corresponding to the metallic ions and core electrons will not be treated explicitly, but will be assumed to give rise to a confinement potential for the conduction electrons, i.e., to specify the geometry of the system. This should be a reasonable starting point to describe simple monovalent metals.) The formulation of electrical transport in terms of the scattering matrix was developed by Landauer²⁴ and Büttiker,²⁵ while the formulation of the statistical mechanics of open quantum systems in terms of the scattering matrix was first given by Dashen, Ma, and Bernstein,²⁶ and was recently revived in the context of the persistent current problem by Akkermans *et al.*²⁷ A unified treatment of the electrical and mechanical properties of metallic nanostructures in terms of the electronic scattering matrix was given by Stafford, Baeriswyl, and Bürki.¹⁵ In the remainder of this section, we recapitulate the general formalism of Ref. 15, which will serve as the starting point for the present investigation.

The essential ingredient in the scattering matrix description of mesoscopic systems is that electrons are injected into the system from *macroscopic* reservoirs in internal thermal equilibrium; any perturbation of the reservoirs due to the mesoscopic current flowing from one to another is assumed to be negligible. The energy distribution of the electrons injected from reservoir α is thus given by the Fermi distribution function $f_\alpha(E) = \{\exp[\beta(E - \mu_\alpha)] + 1\}^{-1}$, where μ_α and $\beta = 1/k_B T$ are the electrochemical potential and inverse temperature, respectively, of reservoir α .

The asymptotic scattering states of conduction electrons for the geometry depicted in Fig. 1 are described by a transverse quantum number ν and a wave number k which is a function of energy E and ν :

$$k_\nu(E) = \sqrt{\frac{2m}{\hbar^2} (E - \epsilon_\nu)}, \quad (1)$$

where ϵ_ν is the energy of the transverse modes. If the amplitudes of incoming currents at energy E are given by a vector with components a_ν^+ (currents from the left side) and a_ν^- (currents from the right side), the outgoing current amplitudes b_ν^+ and b_ν^- are given by

$$\begin{pmatrix} b^+ \\ b^- \end{pmatrix} = S(E) \begin{pmatrix} a^+ \\ a^- \end{pmatrix}. \quad (2)$$

The scattering matrix for a two-terminal conductor may be decomposed into four submatrices

$$S(E) = \begin{pmatrix} S_{11} & S_{12} \\ S_{21} & S_{22} \end{pmatrix}, \quad (3)$$

where the submatrices $S_{ij}(E)$ contain transmission ($i \neq j$) and reflection ($i = j$) amplitudes. Each submatrix $S_{ij}(E)$ is a matrix in the incoming and outgoing scattering channels ν and ν' .

The electrical conductance is given in terms of the scattering matrix by the well-known formula^{24,25}

$$G = \frac{2e^2}{h} \int dE \frac{-\partial f(E)}{\partial E} \text{Tr} \left\{ S_{12}^\dagger(E) S_{12}(E) \right\}, \quad (4)$$

where the factor of 2 accounts for spin degeneracy. Eq. (4) indicates that G is proportional to the sum over the transmission probabilities of electrons incident in a window of width $k_B T$ about the Fermi energy μ . Eq. (4) may be modified by electron-electron interactions at finite temperatures, but has been shown²⁸ to hold quite generally in the limit $T \rightarrow 0$.

The quantity needed to investigate the statistical mechanics of the nanowire is the electronic density of states, $D(E)$. The density of states can be expressed in terms of the scattering matrix as^{26,29}

$$D(E) = \frac{1}{2\pi i} \text{Tr} \left(S^\dagger(E) \frac{\partial S(E)}{\partial E} - \text{h.c.} \right). \quad (5)$$

This expression holds for an arbitrary interacting gas of particles.²⁶ Given the density of states, the grand partition function may be evaluated, and the thermal expectation values of all observables may be calculated.

The expectation value of the total electronic charge on the nanowire is given by

$$\langle Q^- \rangle = -e \int dE f(E) D(E). \quad (6)$$

Integrating by parts, and taking the limit $T \rightarrow 0$, one obtains the simplified expression

$$\langle Q^- \rangle = -\frac{e}{\pi} \text{Im} \{ \ln \det S(E_F) \}. \quad (7)$$

The overall phase of the scattering matrix depends on the exact choice of the asymptotic states (their phase). Therefore the phase relation chosen between the amplitudes a_ν^\pm and b_ν^\pm is in principle free. Different choices correspond to the inclusion of various amounts of the constant asymptotic charge density in Q^- . However, the total charge $Q = \langle Q^- \rangle + Q^+$ is independent of this choice of phase, provided we add the appropriate quantity of the constant positive background charge density.

The grand canonical potential is the relevant thermodynamic potential to describe the mechanical properties of the electron gas in the nanowire, and may be written

$$\Omega = -\frac{1}{\beta} \int dE D(E) \ln(1 + e^{-\beta(E-\mu)}). \quad (8)$$

It should be noted that Eq. (8) only holds for noninteracting electrons, since the thermal trace is taken assuming each fermionic mode is independent. A more general expression for Ω , valid within a self-consistent mean-field treatment of interactions, will be presented elsewhere.³⁰ Here it is sufficient to note that it will be argued below that the corrections to Eq. (8) due to charging effects are negligible.

Eqs. (6) and (8) are deceptively simple, and it is worth emphasizing that μ is the *asymptotic* electrochemical potential of electrons injected from the reservoirs, *not* a local Fermi energy, as introduced by certain other authors.^{18,19} $D(E)$ is the global energy density of eigenstates of the scattering problem, and contains all effects of multiple scattering, quantum interference, etc. These eigenstates are populated according to the Fermi distributions of the reservoirs. The occupation of a local basis of states, which are not eigenstates of H , is in general quite complicated, and will be discussed in detail in Sec. IV E.

In the following, it will be assumed that the volume Ld^2 of the nanowire (or the area Ld for 2D nanowires) remains constant under elongation, *i.e.*, we assume an ideal plastic deformation. It can be shown that relaxation of this constraint, to include *e.g.*, a small elastic deformation, does not modify the mesoscopic effects in an essential way.³⁰ The cohesive force of the nanowire is given by the derivative of the grand canonical potential with respect to the elongation:

$$F = -\frac{\partial \Omega}{\partial L}. \quad (9)$$

Differentiating the above expression for Ω and performing a partial integration over E , one obtains the general result

$$F = \frac{1}{\pi} \int dE f(E) \text{Im} \left\{ \frac{\partial}{\partial L} \ln \det[S(E)] \right\}. \quad (10)$$

We thus have relations which give us the conductance, charge, and force as a function of the S-matrix.

III. THE S-MATRIX OF THE WNW-GEOMETRY

In order to obtain exact results for the tunneling and finite-size corrections to the conducting and thermodynamic properties of metallic nanowires, we consider the special WNW geometry illustrated in Fig. 1, for which the S-matrix can be calculated exactly. The system consists of a noninteracting electron gas confined by hard-wall boundary conditions (we will return to the question of electron-electron interactions in Sec. V B). The wire cross-section in the 3D case is assumed to be square. A generalization to an arbitrary cross section is straightforward if the eigenfunctions and eigenvalues of the 2D Schrödinger equation are known for that shape. The scattering problem for the 2D WNW geometry was solved by Szafer and Stone³¹ in connection with the problem of conductance quantization in 2D semiconductor quantum point contacts, and was further investigated by Weisshaar *et al.*³² In addition to the transmission coefficients calculated in Refs. 31 and 32, we need the reflection coefficients, *i.e.*, the full S-matrix. The generalization of the method of Refs. 31,32 to 3D nanowires and to calculate the full S-matrix is described below.

In order to calculate the elements of the S-Matrix, solutions of the Schrödinger-equation are matched at the transitions between wide and narrow parts of the wire. Let us regard the transition from wide to narrow first (cf. left part of Fig. 1). If the z -coordinate is directed along the wire and x is an abbreviation for x in the two dimensional case and for (x_1, x_2) in the three dimensional case, describing the dimension(s) perpendicular to the z -axis, the wave functions are given by

$$\Psi(z < 0, x) = e^{iK_N z} \Phi_N(x) + \sum_{N'} r_{N'N} e^{-iK_{N'} z} \Phi_{N'}(x), \quad (11)$$

$$\Psi(z > 0, x) = \sum_n t'_{nN} e^{ik_n z} \phi_n(x), \quad (12)$$

where we have assumed an incoming wave from the left of unit amplitude, and Φ_N and ϕ_n are transverse eigenfunctions in the wide and narrow parts of the wire, respectively, and are given by

$$\Phi_N(x) = \sqrt{\frac{2}{D}} \sin\left(\frac{N\pi}{D}(x + D/2)\right) \quad N = 1, 2, \dots \quad (13)$$

$$\phi_n(x) = \sqrt{\frac{2}{d}} \sin\left(\frac{n\pi}{d}(x + d/2)\right) \quad n = 1, 2, \dots \quad (14)$$

in the 2D case, and by an analogous expression consisting of a product of two sine-functions for the 3D case. Here D is the diameter of the wide part of the wire and d the diameter of the narrow part. In the 3D case, the transverse modes have in general two indices, *e.g.*, P and Q , but we can order the states according to their energy and so characterize them by one quantum number N ; P and Q are then functions of N . The wave numbers K_N and k_n are

$$K_N = \sqrt{\frac{2m}{\hbar^2} E - \frac{\pi^2 N^2}{D^2}}, \quad (15)$$

$$k_n = \sqrt{\frac{2m}{\hbar^2} E - \frac{\pi^2 n^2}{d^2}}, \quad (16)$$

where we use the abbreviation (for the 3D case) $N^2 = P(N)^2 + Q(N)^2$.

The solution of the Schrödinger equation must obey two conditions at the transition point $z = 0$:

1. Continuity of the wave function for $x \in [-D/2, D/2]$ in 2D ($x_1, x_2 \in [-D/2, D/2]$ in 3D):

$$\Phi_N(x) + \sum_{N'} r_{N'N} \Phi_{N'}(x) = \sum_n t'_{nN} \phi_n(x) \Theta(d/2 - |x|), \quad (17)$$

where $\Theta(x)$ is the Heavyside step function and is an abbreviation for the product $\Theta(d/2 - |x_1|)\Theta(d/2 - |x_2|)$ in the 3D case.

2. Continuity of the first derivative of the wave function for $x \in [-d/2, d/2]$ in 2D ($x_1, x_2 \in [-d/2, d/2]$ in 3D):

$$K_N \Phi_N(x) - \sum_{N'} r_{N'N} K_{N'} \Phi_{N'}(x) = \sum_n t'_{nN} k_n \phi_n(x). \quad (18)$$

These equations can be transformed into matrix equations for r and t' by multiplication with $\Phi_M(x)$ and $\phi_m(x)$, respectively, and integration over the appropriate x -range. Using the abbreviations

$$\rho_{Nn} = \int_{-d/2}^{d/2} dx \Phi_N(x) \phi_n(x), \quad (19)$$

$$K_{NN'} = \delta_{NN'} K_N, \quad k_{nn'} = \delta_{nn'} k_n, \quad (20)$$

two equations for r and t are obtained:

$$1 + r = \rho t', \quad (21)$$

$$\rho^T K - \rho^T K r = k t'. \quad (22)$$

Note that the ρ matrix is not orthogonal. The equations (21) and (22) can be solved, and we obtain

$$t' = 2(k + \rho^T K \rho)^{-1} \rho^T K, \quad (23)$$

$$r = \rho t' - 1. \quad (24)$$

An exactly analogous calculation for an incoming wave from the right side gives

$$r' = (k + \rho^T K \rho)^{-1} (k - \rho^T K \rho), \quad (25)$$

$$t = \rho + \rho r'. \quad (26)$$

The scattering matrix is obtained by normalizing the wave amplitudes with respect to current (the unitarity of S reflects current conservation). With

$$\bar{t}_{nN} = (k_n/K_N)^{1/2} t_{nN}, \quad \bar{r}_{NN'} = (K_N/K_{N'})^{1/2} r_{NN'}, \quad \text{etc.}, \quad (27)$$

the scattering matrix is given by

$$S^{(1)} = \begin{pmatrix} \bar{r} & \bar{t} \\ \bar{t}' & \bar{r}' \end{pmatrix}. \quad (28)$$

The S–matrix for the combined WNW–geometry may be constructed from three scattering matrices $S^{(1)}$, U , and $S^{(2)}$, describing the scattering at the WN boundary, the free propagation within the narrow section, and the scattering at the NW boundary, respectively (see Fig. 1). The free propagation in the narrow section is described by the matrix

$$U = \begin{pmatrix} 0 & X \\ X & 0 \end{pmatrix}; \quad X_{nn'} = \delta_{nn'} \exp(ik_n L). \quad (29)$$

The NW transition is associated with a matrix

$$S^{(2)} = \begin{pmatrix} \bar{r}' & \bar{t}' \\ \bar{t} & \bar{r} \end{pmatrix}, \quad (30)$$

which can be calculated like $S^{(1)}$, or can be seen by symmetry considerations. To compute the full S–matrix, we use the linear equations connecting the current amplitudes propagating between the individual scattering matrices (see Fig. 1 for an explanation of the notation):

$$\begin{aligned} \begin{pmatrix} b_{S_1}^+ \\ b_{S_1}^- \end{pmatrix} &= S^{(1)} \begin{pmatrix} a_{S_1}^+ \\ a_{S_1}^- \end{pmatrix}, \\ \begin{pmatrix} a_{S_1}^- \\ a_{S_2}^+ \end{pmatrix} &= U \begin{pmatrix} b_{S_1}^- \\ b_{S_2}^+ \end{pmatrix}, \\ \begin{pmatrix} b_{S_2}^+ \\ b_{S_2}^- \end{pmatrix} &= S^{(2)} \begin{pmatrix} a_{S_2}^+ \\ a_{S_2}^- \end{pmatrix}. \end{aligned} \quad (31)$$

Eliminating the unwanted variables in this set of linear equations, and rewriting the equations in the form

$$\begin{pmatrix} b_{S_1}^+ \\ b_{S_2}^- \end{pmatrix} = S \begin{pmatrix} a_{S_1}^+ \\ a_{S_2}^- \end{pmatrix}, \quad (32)$$

relating ingoing and outgoing currents, the full S–matrix is found to be

$$S = P \begin{pmatrix} S_{11}^{(1)} + S_{12}^{(1)}(1 - U_{12}S_{11}^{(2)}U_{21}S_{22}^{(1)})^{-1}U_{12}S_{11}^{(2)}U_{21}S_{21}^{(1)} & S_{12}^{(1)}(1 - U_{12}S_{11}^{(2)}U_{21}S_{22}^{(1)})^{-1}U_{12}S_{12}^{(2)} \\ S_{21}^{(2)}(1 - U_{21}S_{22}^{(1)}U_{12}S_{11}^{(2)})^{-1}U_{21}S_{21}^{(1)} & S_{22}^{(2)} + S_{21}^{(2)}(1 - U_{21}S_{22}^{(1)}U_{12}S_{11}^{(2)})^{-1}U_{21}S_{22}^{(1)}U_{12}S_{12}^{(2)} \end{pmatrix} P. \quad (33)$$

The operator P is a projection operator onto the undamped modes in the wide part of the wire. Note that the individual matrices $S^{(1)}$, $S^{(2)}$, and U are infinite-dimensional matrices describing scattering and propagation in all available modes, including the evanescent modes. The full S–matrix, on the other hand, connects the incoming and outgoing asymptotic states, and thus has a finite dimension for a given energy E , determined by the total number of transverse modes ν with $\epsilon_\nu \leq E$. The inclusion of the virtual intermediate states, which describe tunneling processes, is crucial to solve the Schrödinger equation accurately. However, the contribution of the evanescent modes decreases exponentially with increasing energy. In practice, we found numerical convergence of the S–matrix if roughly 20 times more modes than the undamped modes in the W–part were retained.

We remark that the elements of the S–matrix can also be found by considering *e.g.*, the transmission matrix S_{12} as the sum of the directly transmitted current amplitudes and the multiply backscattered current amplitudes. This results in a geometric series, which can be summed to obtain the result (33).

IV. 2D NANOWIRE

In this section, we investigate the properties of 2D nanowires. There are several motivations to study 2D systems: First, a quasi-2D nanowire could be experimentally realized in a thin metallic film. Secondly, the characteristic electrical and mechanical properties of a nanowire, namely, conductance quantization and force oscillations, are already present in 2D systems, and it is worthwhile to investigate to what extent the universality of the mesoscopic force oscillations predicted in Ref. 15 depends on dimensionality. Further, 2D electronic structure is easier to visualize, making it simple to study the correlations between the measured quantities and the local electronic structure. Finally, and perhaps most importantly, certain of the phenomena studied here are directly applicable to 2D quantum point contacts formed in semiconductor heterostructures.^{7–9} While the predicted mesoscopic force oscillations of order E_F/λ_F would be many orders of magnitude smaller in doped semiconductors due to the smaller Fermi energy and correspondingly longer Fermi wavelength, and would likely be hidden by the much larger cohesive forces associated with the covalently bonded electrons of the valence band, the charge oscillations predicted to accompany the quantized steps in the conductance should have a comparable size in both metallic and semiconductor quantum point contacts, namely, of order the fundamental charge quantum e .

A. Force and conductance

Once the S-matrix (33) is known, the conductance and cohesive force can be calculated from Eqs. (4) and (10). Fig. 2 shows the behavior of the conductance and cohesive force as a function of the elongation of the wire. An ideal plastic deformation of the narrow part is assumed, which means that its area $A = Ld = L_0D$ is held constant, L_0 being the initial length of the narrow section. The wide sections of the wire support 5 propagating modes at the Fermi energy; this fixes the conductance of the wire before deformation to be $G = 5G_0$. In Fig. 2(a), the area of the N-part is comparatively large ($3\lambda_F^2$), while it is small in Fig. 2(b) ($0.5\lambda_F^2$). In both cases, conductance quantization can be observed; whenever a channel in the N-part closes (as the diameter is decreased), the conductance decreases and reaches a plateau at an integer multiple of $2e^2/h$. The conductance does not show a perfect step-like structure, though: When the narrow part is short, there will be tunneling through the constriction before a channel opens, and reflection above the threshold. This will smear out the steps, leading to a rather smooth transition between the plateaus [see Fig. 2(b)]. When the narrow part is quite long, on the other hand, there is almost no tunneling, but a resonant structure near the transition points occurs [Fig. 2(a)]. This is due to the alternating constructive and destructive internal reflection within the constriction.³¹

The cohesive force is strongly correlated with the conductance. In Fig. 2(a), the modulus of the force increases along the conductance plateaus, while it decreases sharply at the conductance steps. The behavior is qualitatively similar to the result for smooth 3D geometries presented in Ref. 15, and to the experimental results for 3D Au nanowires.^{4,5} Thus we see that the essential correlations of the electrical and mechanical properties of nanowires are present even in 2D systems, and even for abrupt geometries. For the extremely short nanowire considered in Fig. 2(b), similar force oscillations correlated with the conductance steps are present (see Fig. 4), but they are superimposed on a much larger background force. The pronounced difference in the force in Figs. 2(a) and 2(b) indicates a breakdown of the invariance of F under a stretching of the geometry $d(z) \rightarrow d(\lambda z)$, which was found within the WKB approximation,¹⁵ due to strong tunneling effects in very short wires.

The cohesive force decays to zero as the wire is elongated past the point where the last conductance channel is cut off, though rather more slowly than the conductance itself. F remains noticeably finite even for the largest elongations shown in Figs. 2(a) and 2(b), although G is exponentially small.³³ The force in this regime arises from the variation of the free energy due to a deformation of the geometry in the region classically forbidden to electrons, and is clearly larger in the shorter wire [Fig. 2(b)], where tunneling effects are more important. This effect is simple to understand: even when the probability to tunnel all the way through the narrow section is exponentially small, the probability to *enter* the narrow section need not be small [see Fig. 5(d)], so the electron gas is still sensitive to its shape.

It is clear from Eq. (10) that all states with energy smaller than the Fermi energy contribute to the total force. On the other hand, the graphs show that the force oscillations are correlated to the behavior of the conductance, and thus must be due to states near the Fermi energy. In Fig. 2(a), one can see that even the resonant structure in the conductance is reflected in the force, leading to sudden changes in its derivative.

Fig. 3 shows the conductance and cohesive force as a function of elongation for wires with different outer diameters. While the curves are distinct at the beginning of the elongation (where inner and outer parts have comparable diameters), there is almost no difference at higher elongations, and this is not only valid for the conductance³² but also for the force. This shows that even a narrow constriction coupled to contacts with infinite width can be accurately modeled by wires of the type we regard here.

B. Mesoscopic force and charge fluctuations

In order to understand the overall behavior of the cohesive force, it is useful to consider a semiclassical expansion^{15,16} of Eq. (8). Formally, the density of states may be written $D(E) = dN(E)/dE$, where $N(E)$ is the total number of states with energy less than E in the system. The behavior of $N(E)$ for 2D domains with hard-wall boundary conditions was first investigated by Weyl,³⁴ and was further developed by Kac and others.^{35,36} The Weyl expansion of $N(E)$ for a 2D domain with a polygonal boundary with n corners is³⁶

$$N(E) = \frac{A}{2\pi} k_E^2 - \frac{\partial A}{2\pi} k_E + 2C + \delta N(E), \quad (34)$$

where $k_E = \sqrt{2mE/\hbar^2}$ is the wavevector associated with energy E , A is the area of the domain, ∂A the circumference of the domain, and C is a constant depending on the topology, in this case

$$C = \sum_{i=1}^n \frac{\pi^2 - \gamma_i^2}{24\pi\gamma_i}, \quad (35)$$

where γ_i is the interior angle of corner i , and $\delta N(E)$ is a fluctuating term associated with the discreteness of the level spectrum, whose energy average is zero.¹⁶ Note that Eq. (34) includes a factor of 2 for spin. The shift in the total number of modes due to the presence of the sharp corners is given by $C = 1/9$ for the WNW geometry of Fig. 1.

Integrating Eq. (8) by parts and taking the limit $T \rightarrow 0$, one finds

$$\Omega = - \int_0^{E_F} N(E) dE = - \frac{\pi E_F}{\lambda_F^2} A + \frac{2E_F}{3\lambda_F} \partial A - 2E_F C + \delta\Omega, \quad (36)$$

where $\delta\Omega$ is a fluctuating mesoscopic correction. Differentiating Ω with respect to L , subject to the constraint $A = \text{const.}$, yields a semiclassical expansion for the force

$$F = - \frac{2E_F}{3\lambda_F} \frac{d}{dL} \partial A + \delta F, \quad (37)$$

where $\delta F = -\partial(\delta\Omega)/\partial L$. The leading order term in the semiclassical expansion of the force is the surface tension, F_{surf} . For the WNW geometry, the circumference of the nanowire is $\partial A = 2L + 2(D - d) + \text{const.}$, and one obtains

$$F_{\text{surf}} = - \frac{4E_F}{3\lambda_F} \left(1 + \frac{d^2}{A} \right). \quad (38)$$

This indicates that the surface tension increases with increasing conductance (the Sharvin formula reads $G/G_0 \sim 2d/\lambda_F$ in 2D) and with *decreasing area* of the wire. The surface tension is plotted in Fig. 2 as a dashed curve. The exact force oscillates around it.

The Weyl expansion for the electronic charge of the nanowire for $T \rightarrow 0$ is

$$\langle Q^- \rangle = -eN(E_F) = -e \left(\frac{2\pi A}{\lambda_F^2} - \frac{\partial A}{\lambda_F} + 2C \right) + \delta Q_0. \quad (39)$$

In Fig. 4, the force fluctuations δF , calculated by subtracting the surface tension from the exact force, and the charge fluctuations δQ_0 , calculated by subtracting the term in parentheses in Eq. (39) from the exact charge, determined from Eq. (7), are shown for the nanowires considered in Fig. 2. The scale of the force oscillations is E_F/λ_F (see Fig. 4), similar to the result for smooth 3D geometries presented in Ref. 15. Strongly correlated with the force oscillations are charge oscillations of order the fundamental charge quantum e . The charge fluctuations δQ_0 are calculated in the absence of screening. Screening will be considered in Sec. VB; here it suffices to note that the screening properties of the 2D electron gas in *e.g.* GaAs are quite poor, so that the charge fluctuations in small-conductance 2D quantum point contacts should be essentially unscreened. The predicted charge oscillations should be experimentally observable with a local probe, such as a single-electron transistor.

C. Topological force

A close examination of Fig. 2 indicates that the exact force deviates significantly from the surface tension for very small elongations: The discrepancy is roughly $3E_F/\lambda_F$ in Fig. 2(a) and $14E_F/\lambda_F$ in Fig. 2(b) for $L \rightarrow L_0$. This behavior is to be contrasted with the results for smooth geometries, presented in Ref. 15, in which the mesoscopic deviations from the semiclassical result were always found to be $\lesssim E_F/\lambda_F$ (hence the term *universal*). The nonuniversal corrections to the force in the WNW geometry at small deformations have a topological origin: Before deformation, the perfect wire has a smooth boundary, but as the wire is stretched, eight sharp corners develop. The sharp corners lead to a shift in the grand canonical potential

$$\Delta\Omega_{\text{top}} = -2E_FC = -\frac{2}{9}E_F. \quad (40)$$

However, the electrons incident from the reservoirs can only resolve the individual corners when they are separated by a distance greater than or of order λ_F . Thus one may expect the topological correction to Ω due to the sharp corners to evolve smoothly with the initial deformation, and to saturate when the corners become separated by an amount of order λ_F . In order to see this explicitly, let us consider $\Delta\Omega_{\text{top}}$ as the work done by a topological force $F_{\text{top}} = F - F_{\text{surf}}$ which is present for small deformations $L \approx L_0$. For infinitesimal deformations, the adiabatic approximation becomes exact, and gives $F(L_0) = -4E_F/3\lambda_F$. Thus $F_{\text{top}}(L_0) = 4E_FD/3\lambda_FL_0$. Estimating the work done by F_{top} to be $-F_{\text{top}}(L_0)\Delta L/2$, and equating this to the change in the grand canonical potential $\Delta\Omega_{\text{top}}$, gives $\Delta L = \lambda_FL_0/3D$ as the deformation regime where the topological force is important. The corresponding change in diameter is

$$\Delta d = -D\Delta L/L_0 = -\lambda_F/3, \quad (41)$$

indicating that the shift in the free energy of the system due to the introduction of sharp corners indeed saturates when the separation between the corners becomes comparable to the Fermi wavelength. That the force associated with this change of topology can be large compared to E_F/λ_F is a remarkable result.

D. Comparison with the adiabatic approximation

In previous theoretical investigations of the conductance and cohesive force in metallic nanowires, an adiabatic approximation¹⁵ was employed. The WNW geometry clearly violates the conditions of validity of the adiabatic approximation; it is nonetheless instructive to compare our exact results to those obtained within an adiabatic approximation for this abrupt geometry, in order to evaluate the importance of interchannel scattering.

The solution of the 2D Schrödinger equation can be written formally as $\Psi(x, z) = \phi_z(x)\psi(z)$. The adiabatic approximation consists of neglecting the derivatives $\partial\phi_z(x)/\partial z$ and $\partial^2\phi_z(x)/\partial z^2$ (which would be justified if $|\partial D(z)/\partial z| \ll 1$), so that the Schrödinger equation decouples into separate transverse and longitudinal wave equations,

$$-\frac{\hbar^2}{2m}\frac{\partial^2}{\partial x^2}\phi_z^\nu(x) = E_\nu(z)\phi_z^\nu(x), \quad (42)$$

$$-\frac{\hbar^2}{2m}\frac{\partial^2}{\partial z^2}\psi(z) = (E - E_\nu(z))\psi(z). \quad (43)$$

The 2D scattering problem then decouples into independent one-dimensional scattering problems for each channel, and the scattering matrix reduces to a 2×2 matrix for each channel, which can be computed *e.g.*, via the WKB approximation.¹⁵ It is then straightforward to calculate conductance and cohesive force using the formalism described in Sec. II.

While the adiabatic approximation should be a good approximation for boundaries with smoothly varying diameter, this condition is certainly not fulfilled in the WNW-geometry. Employing it nonetheless, the equation of motion for the longitudinal coordinate becomes just the 1D Schrödinger equation for a square barrier:

$$\left(-\frac{\hbar^2}{2m}\frac{\partial^2}{\partial z^2} + \theta(z)\theta(L-z)V_\nu\right)\phi(z) = \tilde{E}_\nu\phi(z) \quad (44)$$

with $V_\nu = E_F\frac{\pi^2\nu^2}{k_F^2}\left(\frac{1}{d^2} - \frac{1}{D^2}\right)$ and $\tilde{E}_\nu = E - E_F\frac{\pi^2\nu^2}{k_F^2D^2}$. The transmission and reflection coefficients are simply calculated using the continuity of the wave function and its derivative at the potential steps. We find

$$\begin{aligned}
r_\nu &= \frac{(1 - e^{2ik_\nu L})(k_\nu^2 - K_\nu^2)}{-k_\nu^2 + e^{2ik_\nu L}k_\nu^2 - 2k_\nu K_\nu - 2e^{2ik_\nu L}k_\nu K_\nu - K_\nu^2 + e^{2ik_\nu L}K_\nu^2}, \\
t_\nu &= \frac{-4e^{ik_\nu L}k_\nu K_\nu}{-k_\nu^2 + e^{2ik_\nu L}k_\nu^2 - 2k_\nu K_\nu - 2e^{2ik_\nu L}k_\nu K_\nu - K_\nu^2 + e^{2ik_\nu L}K_\nu^2},
\end{aligned} \tag{45}$$

where $K_\nu = k_F \sqrt{\tilde{E}_\nu/E_F}$ and $k_\nu = k_F \sqrt{(\tilde{E}_\nu - V_\nu)/E_F}$.

Inserting the S-matrix elements (45) into Eqs. (4) and (10), one obtains the adiabatic approximation for the conductance and force. These are shown as dotted curves in Fig. 2. The adiabatic approximation captures some of the qualitative features of the exact solution (solid curves), but is not quantitatively correct. Since the conductance is more or less quantized, the discrepancy with respect to the exact solution has to be small. Not so for the force; the adiabatic approximation clearly fails to describe correctly even the leading order contribution to the force, the surface tension, when several channels are transmitted, especially for very short nanowires. Interestingly, the adiabatic approximation *overestimates* the effects of tunneling: both the conductance plateaus and the force oscillations are better defined in the exact calculation than in the adiabatic approximation. Perhaps the most striking conclusion that one should draw from Fig. 3 is that even for the worst-case scenario of an abrupt geometry, the adiabatic approximation works remarkably well for nanowires of length $L \gg \lambda_F$.

E. Local density of states

The correlations between the quantized steps in the conductance and the oscillations of order E_F/λ_F in the force were interpreted in Ref. 15 in terms of a simple physical picture, which was essentially the converse of the conventional interpretation. The conventional interpretation^{21–23} of the experiments of Refs. 4,5 is that the jumps in the conductance are due to abrupt changes of the structure of the nanowire at the atomic level, *e.g.*, through the breaking of bonds, and that these structural rearrangements manifested themselves as abrupt changes in the cohesive force. While certainly a plausible viewpoint, the strong statistical evidence^{2,3,6} for *conductance quantization* has no natural explanation within this framework. In order to substantiate the converse point of view, that the conductance channels themselves can be interpreted as mesoscopic bonds providing the cohesion, it is worthwhile investigating the local electronic structure of a nanowire within the jellium model.

The electrical conductance is determined by the electronic structure of the nanowire in the vicinity of the Fermi energy. While the total force and charge clearly depend on all the states with energy below E_F [*c.f.*, Eqs. (6) and (10)], the mesoscopic force and charge oscillations, because they are correlated with the conductance steps, must also be essentially determined by the electronic states at the Fermi energy. The spatial character of the electronic wavefunctions associated with scattering states of a given energy E is naturally represented through the local density of states (LDOS), $D(E, x, z)$. The LDOS of 2D quantum point contacts with smooth boundaries has recently been investigated by Ulreich and Zwirger.³⁷

While Refs. 18–20 regarded the density of states to be independent of the z -coordinate and to depend only on the x -coordinate in the narrow part of the wire, this is certainly not the case for the full solution of the problem. The z -dependence of the LDOS will be especially important when not only the width but also the length of the nanowire are on the nanometer scale, as in the experimentally relevant geometry. Since we know the exact S-matrix and the eigenfunctions for the WNW geometry, we can calculate the LDOS. The LDOS is obtained as a sum of the densities created by the different incoming channels. Only reflected or transmitted waves from the same channel will superpose coherently. In the wide section on the left side of the constriction, the LDOS at the Fermi energy is given by

$$\begin{aligned}
D(E, x, z < 0) &= \frac{2}{\hbar} \sum_{N=1}^{N_{\max}} \left\{ \left| \frac{e^{iK_N z}}{\sqrt{\hbar K_N/m}} \Phi_N(x) + \sum_{N'=1}^{\infty} (S_{11})_{N'N} \frac{e^{-iK_{N'} z}}{\sqrt{\hbar K_{N'}/m}} \Phi_{N'}(x) \right|^2 \right. \\
&\quad \left. + \left| \sum_{N'=1}^{\infty} (S_{12})_{N'N} \frac{e^{-iK_{N'} z}}{\sqrt{\hbar K_{N'}/m}} \Phi_{N'}(x) \right|^2 \right\},
\end{aligned} \tag{46}$$

where S_{ij} are the submatrices of the S-matrix (3), and we have chosen $z = 0$ at the boundary between wide and narrow parts. For the calculation of the LDOS in the narrow part of the wire, we need the current amplitudes $b_{S_1}^-$ and $b_{S_2}^+$ in the narrow section as a function of the incoming current amplitudes $a_{S_1}^+$ and $a_{S_2}^-$ (see Fig. 1). In the system of linear equations (31), the unwanted variables have to be eliminated, and the remaining equations may be rewritten as

$$\begin{pmatrix} b_{S_1}^- \\ b_{S_2}^+ \end{pmatrix} = t \begin{pmatrix} a_{S_1}^+ \\ a_{S_2}^- \end{pmatrix}. \quad (47)$$

We find

$$t = \begin{pmatrix} t_{11} & t_{12} \\ t_{21} & t_{22} \end{pmatrix} \quad (48)$$

with the components of t given by the known matrices $S^{(1)}$ (28), $S^{(2)}$ (30) and U (29) as

$$t_{11} = \left(1 - S_{22}^{(1)} U_{12} S_{11}^{(2)} U_{21}\right)^{-1} S_{21}^{(1)}, \quad (49)$$

$$t_{12} = S_{22}^{(1)} U_{12} \left(1 - S_{11}^{(2)} U_{21} S_{22}^{(1)} U_{12}\right)^{-1} S_{12}^{(2)}, \quad (50)$$

$$t_{21} = \left(1 - S_{11}^{(2)} U_{21} S_{22}^{(1)} U_{12}\right)^{-1} S_{11}^{(2)} U_{21} S_{21}^{(1)}, \quad (51)$$

$$t_{22} = \left(1 - S_{11}^{(2)} U_{21} S_{22}^{(1)} U_{12}\right)^{-1} S_{12}^{(2)}. \quad (52)$$

The LDOS in the narrow part of the wire is obtained as

$$D(E, x, 0 < z < L) = \frac{2}{\hbar} \sum_{N=1}^{N_{\max}} \left\{ \left| \sum_{n'=1}^{\infty} \left[(t_{11})_{n'N} \frac{e^{ik_{n'}z}}{\sqrt{\hbar k_{n'}/m}} \phi_{n'}(x) + (t_{21})_{n'N} \frac{e^{-ik_{n'}(z-L)}}{\sqrt{\hbar k_{n'}/m}} \phi_{n'}(x) \right] \right|^2 + \left| \sum_{n'=1}^{\infty} \left[(t_{12})_{n'N} \frac{e^{ik_{n'}z}}{\sqrt{\hbar k_{n'}/m}} \phi_{n'}(x) + (t_{22})_{n'N} \frac{e^{-ik_{n'}(z-L)}}{\sqrt{\hbar k_{n'}/m}} \phi_{n'}(x) \right] \right|^2 \right\}. \quad (53)$$

The LDOS is of course symmetric about the axis $z = L/2$.

Fig. 5 shows the LDOS at the Fermi energy for 4 different elongations of a wire with a relatively long N-part (it has the same parameters as the wire in Fig. 2(a), so one can compare the conductance and force at these elongations with the LDOS). It can be seen immediately that the LDOS exhibits a highly nontrivial structure. The number of maxima in x -direction in the N-part of the wire reflects the number of open channels transmitted through the constriction; in Fig. 5(a) there are three open channels (and thus $G \approx 3G_0$ see fig. 2), in (b) there are two open channels and in (c) only one channel is left. Fig. 5(d) shows the exponential damping of the wave function just after the last channel has closed. So the highest open mode dominates the transverse structure in the LDOS in the narrow part of the wire; this can be understood considering that normalization of the wavefunctions to unit current implies that the wavefunctions are proportional to $1/\sqrt{d-d_n}$, where d_n is the wire diameter at which the n th channel opens. Note that even in the tunneling regime [Fig. 5(d)], the probability for an electron to enter the classically forbidden region can be non-negligible.

As the conductance is a property of states at the Fermi energy, we should expect not only the number of transmitted channels to be reflected in the LDOS, but also the resonant structure exhibited by the conductance in Fig. 2(a). This is indeed the case; when we are at conductance maxima, the LDOS inside the N-part is much larger than that at the minima, and is very strongly modulated in the z -direction. This is because constructive interference of the multiply backscattered waves leads to a quasi-bound standing-wave state at the conductance maxima, while the conductance minima are associated with a condition of destructive interference [compare Fig. 5(b) (conductance minimum) and Fig. 5(c) (conductance maximum)]. For the first conductance maximum after the channel opens as one widens the narrow section, there is one maximum in the LDOS of the N-part in the longitudinal direction; for the n th conductance maximum of the resonant structure, there are n longitudinal maxima of the LDOS. We thus see 5 maxima in Fig. 5(c).

The electronic structure of the nanowire shown in Fig. 5 gives vivid pictorial support to the claim advanced in Ref. 15 that conductance channels should be interpreted as mesoscopic bonds, which provide the cohesion of the system. The claim advanced here that the electronic structure in such a nanowire is dominated by quantum-confinement effects rather than by atomistic effects is in agreement with STM studies of electron ‘‘corrals’’ on Cu surfaces.³⁸

V. 3D NANOWIRE

While the results for 2D nanowires presented in the preceding section are interesting both in illustrating the generality of the mesoscopic phenomena in question and for their relevance to experiments on point contacts in quasi-2D electron gases, the only experiments to date on the mechanical properties of nanowires^{4,5} involve 3D metals. In

this section, we consider a 3D wire with WNW–geometry and square cross–section. For a square cross section, many modes are doubly degenerate, as in the case of cylindrical symmetry, leading to conductance steps of both $2e^2/h$ and $4e^2/h$. It would be possible to lift this degeneracy by considering a wire with a rectangular rather than square cross–section. The formalism to compute the S–matrix (cf. Sec. III) and to obtain the force, charge, and conductance (see Sec. II) is the same as in the 2D case, although one needs to include more evanescent modes for an accurate computation of the S–matrix than in the 2D case. It is straightforward to extend the present calculation to wires of arbitrary cross–section, if the eigenfunctions and eigenvalues of the 2D Schrödinger equation are known for that cross–section.

Although the exactly solvable geometry considered here is somewhat special due to the presence of sharp edges, the gross behavior of the conductance and force is similar to that observed experimentally in 3D metallic nanowires^{4,5} and calculated for smooth, adiabatic geometries.¹⁵ The agreement of the present results for the WNW geometry with the experimental results of Ref. 4 is poorer than for the smooth geometries considered previously,¹⁵ indicating that the experimental geometry is undoubtedly much smoother than that considered here.

A. Force and Conductance

Fig. 6 shows the conductance and tensile force as a function of elongation for two model 3D wires. Under elongation, the narrow section is assumed to deform plastically, *i.e.*, its volume $V = Ld^2 = L_0D^2$ is held constant, where L_0 is the initial length of the narrow section. The inclusion of an additional, small elastic deformation can be shown not to modify the mesoscopic effects in an essential way.³⁰ The comparison of the exact results shown here to the results of an adiabatic approximation is similar to that in the 2D case (c.f. Fig. 2), so for clarity we have not shown them for the 3D case.

In Fig. 6(a), a nanowire with a volume of $4\lambda_F^3$ is shown, while a shorter wire with a volume of $1.25\lambda_F^3$ is shown in Fig. 6(b). The width of the wide sections is $D = 1.76\lambda_F$, which fixes the number of asymptotic propagating modes to be 6. In Fig. 6(a), one sees conductance plateaus at $G = 1, 3, 4, 6 \times G_0$, with a pronounced resonant structure superimposed due to multiple reflection at the abrupt junctions between wide and narrow sections. The sequence of degeneracies corresponds to the square symmetry of the cross–section (cylindrical symmetry, on the other hand, gives $G = 1, 3, 5, 6, \dots \times G_0$, see Ref. 15). Just as in the 2D case discussed above, the force exhibits mesoscopic oscillations of order E_F/λ_F , which are correlated with the conductance steps: $|F|$ increases along the conductance plateaus, and drops abruptly at the conductance steps. The resonant structure in the conductance is also reflected in the first derivative of the force, particularly on the last conductance plateau. The force is similar in magnitude to that calculated for a smooth geometry in Ref. 15 and observed experimentally in Au nanowires in Ref. 4: the forces required to cut off the last two conductance eigenmodes are of order $1.25E_F/\lambda_F$ and $2.5E_F/\lambda_F$, respectively (recall that $E_F/\lambda_F \approx 1.7\text{nN}$ in Au).

The surface tension has been plotted for comparison as a dashed curve in Fig. 6. It has been computed analogously to the 2D case from the Weyl expansion^{15,16} of the grand canonical potential,

$$\Omega = -E_F \left(\frac{16\pi}{15\lambda_F^3} V - \frac{\pi}{4\lambda_F^2} \partial V + \frac{2}{3\lambda_F} \sum_{\text{edges } i} C_i L_i \right) + \delta\Omega, \quad (54)$$

where V is the volume and ∂V the surface area of the nanowire; the topological terms are proportional to the lengths of the edges L_i , and the appropriate constants are $C_i = 1/4$ for an edge with an inner angle of $\pi/2$ and $C_i = -5/36$ for an edge with an inner angle of $3\pi/2$. The surface tension, or semiclassical approximation to the force, is obtained from the derivative of the semiclassical approximation to Ω [the term in parentheses in Eq. (54)] with respect to L , which yields

$$F_{\text{surf}} = -\frac{E_F}{\lambda_F} \left(\frac{\pi d}{2\lambda_F} + \frac{\pi d^2}{2L\lambda_F} - \frac{2}{3} - \frac{d}{2.7L} \right) \quad (55)$$

for a 3D nanowire with WNW geometry and square cross–section. Aside from the initial deformation, where the topological force is important (c.f. Sec. IV B), the force exhibits oscillations centered about the semiclassical result (dashed curve).

In Fig. 6(b), a shorter wire whose conductance versus elongation matches the experimental curve shown in Fig. 1 of Ref. 4 is shown; L_0 was chosen such that the elongation required to decrease the conductance from $6G_0$ to 0 is $2\lambda_F \approx 1\text{nm}$. We see that the conductance and force are correlated in a similar way. Due to the shorter length of the constriction, the conductance steps are smeared out by tunneling and by above-threshold reflection; the plateau at

$G = 4G_0$ and the associated structure in the force are no longer visible. The resonant structure in the conductance is also suppressed, except on the last plateau, where the narrow section is longest. The overall magnitude of the force is larger than for longer constrictions, due to the increased surface tension, and the total elongation required to break the nanowire is less. (Note that the effective surface tension can be reduced by up to a factor of 5 by including a small elastic deformation.³⁰) However, the oscillations of the force around the semiclassical approximation are of the same order as in the previous case (see Fig. 7). The pronounced difference in Figs. 6(a) and 6(b) indicates a breakdown of the invariance of F under a stretching of the geometry $d(z) \rightarrow d(\lambda z)$, which was found within the WKB approximation,¹⁵ due to strong tunneling effects in very short wires.

As in the 2D case, the force decays to zero with increasing elongation after the last conductance channel is cut off, although more slowly than does the conductance itself (see Sec. IV A for a discussion). F remains non-negligible even for the largest elongations shown in Fig. 6, when the conductance is exponentially small.³³ A similar effect was observed experimentally (c.f. Fig. 1 of Ref. 4), although it is not clear whether the effect was above the noise level.

B. Charge oscillations and screening

The charge on such a 3D nanowire may be calculated from Eq. (7), as in the 2D case. The charge on the nanowire changes as the wire is elongated due to surface terms and mesoscopic oscillations. The Weyl expansion for the electronic charge of the nanowire is

$$\langle Q^- \rangle = -e \left(\frac{8\pi}{3\lambda_F^3} V - \frac{\pi}{2\lambda_F^2} \partial V + \frac{1}{\lambda_F} \sum_{\text{edges } i} C_i L_i \right) + \delta Q_0, \quad (56)$$

The term in parentheses in Eq. (56) varies smoothly as the geometry of the wire is altered, while δQ_0 describes the mesoscopic oscillations associated with the opening or closing of discrete transverse modes.

In Fig. 7, the mesoscopic charge oscillations δQ_0 , calculated by subtracting the term in parentheses in Eq. (56) from the exact charge computed via Eq. (7), and the force oscillations, calculated by subtracting the surface tension from the total force, are plotted for both wires shown in Fig. 6 as a function of elongation. As in the 2D case, there is a strong correlation between the two quantities, and the charge oscillations are of order the fundamental quantum of charge e . The force oscillations are, as in the case of an adiabatic geometry studied in Ref. 15, of order E_F/λ_F , aside from the nonuniversal topological correction occurring for small deformations from an ideal wire, which was discussed in detail for the 2D case in Sec. IV C.

In an interacting system, screening of the charge oscillations will occur. The net charge δQ including screening can be estimated within the Thomas-Fermi approximation as follows:

$$\delta Q = \delta Q_0 - e^2 D(E_F) \delta V, \quad (57)$$

where δQ_0 are the charge oscillations in the noninteracting case regarded above, $D(E)$ is the density of states (integrated over the length of the constriction) and the potential δV due to the charge imbalance on the wire can be estimated as

$$\delta V = \frac{\delta Q}{C}. \quad (58)$$

We have introduced a phenomenological quantity C corresponding to the total capacitance of the inner part of the wire to its surroundings. Eqs. (57) and (58) can be used to compute self-consistently the charge on the wire within linear response:

$$\delta Q = \frac{\delta Q_0}{1 + e^2 D(E_F)/C}. \quad (59)$$

The charge in the noninteracting case δQ_0 has already been computed and discussed (see Fig. 7).

On dimensional grounds, the capacitance obeys $C = \alpha L$, where α is a geometrical constant of order 1 (α may depend logarithmically on the ratio D/L). The density of states can be computed by a spatial integral of the LDOS over the narrow section, or from the asymptotic scattering phase shifts via Eq. (5). The later definition includes the contribution of the Friedel oscillations induced in the wide sections. In Fig. 8, both densities of states are shown for wires with the same parameters as above. They are approximately equal, indicating that the excess charge δQ induced on the nanowire under deformation resides mainly on the narrow section. The intricate resonant structure

in $D(E_F)$ occurs due to the formation of quasi-bound states due to multiple reflection at the junctions of the wide and narrow sections (see Fig. 5), and would not be present for a smooth geometry, such as that studied in Ref. 15. Aside from this resonant structure, the overall magnitude of $D(E_F)$ can also be determined from a Weyl expansion. To leading order, one finds $D(E_F) \sim (4L/E_F\lambda_F)G/G_0$. Inserting this expression into Eq. (59), one finds

$$\delta Q \sim \frac{\delta Q_0}{1 + 0.66r_s G/G_0\alpha}, \quad (60)$$

where r_s is the dimensionless electron gas parameter, which takes values between 2 and 6 in metals. This indicates that the screening of the mesoscopic charge fluctuations is poor for wires with small conductance. The screened mesoscopic charge fluctuations should be measurable with a local probe, such as a single-electron transistor.

The screening of the predicted charge fluctuations should be even weaker in 2D GaAs quantum point contacts, due to the large dielectric constant, which enhances the capacitance. In the 2D case, the constant 0.66 is replaced by 0.52 in the denominator of Eq. (60), and the geometrical factor $\alpha \rightarrow \varepsilon\alpha$, where $\varepsilon \approx 13$. This indicates that the predicted charge fluctuations are essentially unscreened for small-conductance QPCs in GaAs.

Let us finally add a comment on the effect of screened electron-electron interactions on the free energy. Within linear response, the Coulomb energy associated with the mesoscopic charge imbalance is given by

$$\Delta\Omega_C = \frac{1}{2} \int d^3x \vec{D} \cdot \vec{E}. \quad (61)$$

In the discrete potential model introduced above to treat screening, this leads to

$$\Delta\Omega_C = \frac{\delta Q_0^2}{C + e^2 D(E_F)}. \quad (62)$$

The details of the derivation of Eq. (62) will be given elsewhere.³⁰ Equation (62) indicates that the mesoscopic charge fluctuations of order e lead to a negligible correction to the free energy of the system, even in the limit $C \rightarrow 0$ of perfect screening, justifying the independent-electron model of nanocoherence.

VI. CONCLUSIONS

In the present article, we have investigated the conducting and thermodynamic (including mechanical) properties of metallic nanowires with a wide–narrow–wide geometry, using a free-electron model with hard-wall boundary conditions. All properties of the nanowire were related to the electronic scattering matrix, which was evaluated exactly, including all effects of tunneling and interchannel scattering. The present results confirm the central conclusion of Ref. 15, which was based on an evaluation of the scattering matrix within the adiabatic and WKB approximations, that closing a conductance channel by stretching a metallic nanowire requires a force of order E_F/λ_F , or roughly a nanonewton in monovalent metals, independent of the total number of conducting channels.

In contrast to this “universal” behavior under a smooth deformation of the geometry, we have shown that the force associated with a change in topology can be large compared to E_F/λ_F , and indeed comparable to the total (macroscopic) cohesive force.

In addition, we predict that the net charge on a nanowire exhibits oscillations of order the fundamental charge quantum e , which are synchronized with the force oscillations and conductance steps. These charge oscillations should also be present in quasi-2D quantum point contacts in GaAs heterostructures, and should be experimentally detectable using a local probe, such as a single-electron transistor.

A final word should be added by way of addressing the central controversy of this field, which can be stated as follows: Is it the atomic structure (*i.e.*, the bonds) which determines the conductance,^{21–23,39} or should the conductance channels themselves be thought of as mesoscopic bonds which provide the cohesion, and thus determine the structure?

The conductance channels are the eigenstates of the electronic scattering problem,⁴⁰ and are thus the appropriate states to describe both the transport and thermodynamic properties of a nanowire, which is an open quantum mechanical system. These scattering states are linear combinations of local bonding states, so there is no fundamental contradiction between the two viewpoints stated above: one is free to look at the problem in a localized basis of bonds or in a basis of extended electronic eigenstates.

However, since an exact solution of the many-body Schrödinger equation for a nanowire is beyond our current capabilities, one is forced to make certain approximations, which are convenient in the basis of choice. Thus molecular dynamics simulations^{21–23} typically neglect any quantum coherence between different bonds, and amount to a

computational version of the classical ball-and-stick model of atomic structure, where bonds are described by a short-ranged empirical inter-atomic potential. This is an uncontrolled approximation, which should be adequate to describe covalent bonds in an insulator, but its applicability for monovalent metals with nearly spherical Fermi surfaces like Au and Na is questionable.

The molecular dynamics simulations involve empirically determined short-range interatomic potentials whose characteristic length and energy scales mimic the quantum mechanics of bonding. When playing classical mechanics with these quantum forces, it is not too surprising if one obtains forces of the right order of magnitude. Such models are of course inadequate to describe electrical conduction, so to explain the observed correlations in the conductance and force of metallic nanowires, a quantum-mechanical model whose geometry is fit to the results of the classical simulation is constructed.^{21–23} The cost of working in a localized basis is thus the necessity of using *different physical laws* to describe conductance and cohesion.

On the other hand, we have seen in the present article (see also Ref. 15) that the observed correlations in the conducting and mechanical properties of metallic nanowires can be accounted for naturally in a *single* quantum mechanical model, which treats the mechanical and electrical properties of the system on an equal footing. In order to solve the quantum scattering problem, we have neglected the discrete atomic structure, working in a jellium-like model, which is equivalent to assuming that the only effect of the lattice is to modify the electron’s effective mass. This should be a rather good approximation for simple metals like Na and adequate for noble metals like Au. Defects in the atomic structure of the wire or roughness in its surface introduce additional scattering, which can also be included in the jellium model in a natural way.¹² A drawback of the jellium model, or at least of the assumption employed here and in Ref. 15 that the positive background deforms continuously as the nanowire is elongated, is the inability to describe the hysteretic behavior found in the experiment of Ref. 4. The claim advanced here that the electronic structure in such a nanowire is dominated by quantum-confinement effects rather than by atomistic effects is in agreement with STM studies of electron “corrals” on Cu surfaces.³⁸

In the end, the merits of the jellium model vis à vis an atomistic description must be decided based on its predictive power. An interesting prediction of the jellium model discussed above is the existence of mesoscopic charge fluctuations of order e , which are strongly correlated with the force fluctuations, and synchronized with the conductance steps. These charge fluctuations are a collective effect, which can not be described in a ball-and-stick picture of bonding. It is incumbent on the experimenter to verify or falsify this clear prediction of the jellium model.

ACKNOWLEDGEMENTS

C. A. S. acknowledges valuable discussions with J. Bürki and D. Baeriswyl. This work was supported in part by the Deutsche Forschungsgemeinschaft through grant SFB 276.

* Present address.

¹ For a general reference, see *Nanowires*, P. A. Serena and N. García eds. (Kluwer Academic Publishers, Dordrecht, 1997).

² L. Olesen, E. Lægsgaard, I. Stensgaard, F. Besenbacher, J. Schiøtz, P. Stoltze, K. W. Jacobsen, and J. K. Nørskov, *Phys. Rev. Lett.* **72**, 2251 (1994); *ibid.*, **74**, 2147 (1994).

³ J. M. Krans, J. M. van Ruitenbeek, V. V. Fisun, I. K. Yanson, and L. J. de Jongh, *Nature* **375**, 767 (1995).

⁴ C. Rubio, N. Agraït, and S. Vieira, *Phys. Rev. Lett.* **76**, 2302 (1996); C. Untiedt, G. Rubio, S. Vieira, and N. Agraït, *Phys. Rev. B* **56**, 2154 (1997).

⁵ A. Stalder and U. Dürig, *Appl. Phys. Lett.* **68**, 637 (1996); *J. Vac. Sci. Technol. B* **14**, 1259 (1996).

⁶ J. L. Costa-Krämer, N. García, and H. Olin, *Phys. Rev. B* **55**, 12910 (1997).

⁷ B. J. van Wees, H. van Houten, C. W. J. Beenakker, J. G. Williamson, L. P. Kouwenhoven, D. van der Marel, and C. T. Foxon, *Phys. Rev. Lett.* **60**, 848 (1988).

⁸ D. A. Wharam, T. J. Thornton, R. Newbury, M. Pepper, H. Ahmed, J. E. F. Frost, D. G. Hasko, D. C. Peacock, D. A. Ritchie, and G. A. C. Jones, *J. Phys. C* **21**, L209 (1988).

⁹ For a review, see C. W. J. Beenakker and H. van Houten, in *Solid State Physics: Advances in Research and Applications*, H. Ehrenreich and D. Turnbull eds. (Academic Press, New York, 1991) Vol. 44, p. 1.

¹⁰ E. Bascones, G. Gómez-Santos, and J. J. Sáenz, *Phys. Rev. B* **57**, 2541 (1998).

¹¹ P. García-Mochales and P. A. Serena, *Phys. Rev. Lett.* **79**, 2316 (1997).

¹² J. Bürki, C. A. Stafford, X. Zotos, and D. Baeriswyl (unpublished).

¹³ D. L. Maslov, C. Barnes, and G. Kirczenow, *Phys. Rev. Lett.* **70**, 1984 (1993); *Phys. Rev. B* **48**, 2543 (1993); C. W. J. Beenakker and J. A. Melsen, *Phys. Rev. B* **50**, 2450 (1994).

- ¹⁴ S. Das Sarma and S. He, *Int. J. Mod. Phys. B* **7**, 3375 (1993).
- ¹⁵ C. A. Stafford, D. Baeriswyl, and J. Bürki, *Phys. Rev. Lett.* **79**, 2863 (1997).
- ¹⁶ C. Höppler and W. Zwerger, *Phys. Rev. Lett.* **80**, 1792 (1998).
- ¹⁷ C. A. Stafford, *Physica E* **1**, 310 (1998).
- ¹⁸ J. M. van Ruitenbeek, M. H. Devoret, D. Esteve, and C. Urbina, *Phys. Rev. B* **56**, 12566 (1997).
- ¹⁹ A calculation similar to that of Ref. 18, with screening treated in the spirit of the Thomas-Fermi approximation, is given by C. Yannouleas and U. Landman, *J. Phys. Chem. B* **101**, 5780 (1997); the connection of the nanowire to the electrodes is not considered. A subsequent treatment of a nanowire of nonuniform cross section in the adiabatic approximation is presented by C. Yannouleas, E. N. Bogachek, and U. Landman, *Phys. Rev. B* **57**, 4872 (1998); however, mesoscopic corrections to the charge density are neglected in the treatment of screening. In fact, the results for the mesoscopic force oscillations are essentially equivalent to those for the free-electron model, presented previously in Ref. 15.
- ²⁰ S. Blom, H. Olin, J. L. Costa-Krämer, N. Garcia, M. Jonson, P. A. Serena, and R. I. Shekhter, *Phys. Rev. B* **57**, 8830 (1998), derive an expression for the grand canonical potential Ω of a nanowire which is a special case of that given in Ref. 15 for the case $D(z) = \text{constant}$. However, the connection of the nanowire to the electrodes is not considered.
- ²¹ U. Landman, W. D. Luedtke, N. A. Burnham, and R. J. Colton, *Science* **248**, 454 (1990); U. Landman, W. D. Luedtke, B. E. Salisbury, and R. L. Whetten, *Phys. Rev. Lett.* **77**, 1362 (1996).
- ²² T. N. Todorov and A. P. Sutton, *Phys. Rev. Lett.* **70**, 2138 (1993); *Phys. Rev. B* **54**, R14234 (1996).
- ²³ M. R. Sørensen, M. Brandbyge, and K. W. Jacobsen, *Phys. Rev. B* **57**, 3283 (1998).
- ²⁴ R. Landauer, *IBM J. Res. Dev.* **1**, 223 (1957); *Phil. Mag.* **21**, 863 (1970).
- ²⁵ M. Büttiker, *Phys. Rev. Lett.* **57**, 1761 (1986); in *Nanostructured Systems*, M. Reed ed., p. 191 (Academic Press, New York, 1992).
- ²⁶ R. Dashen, S.-K. Ma, and H. J. Bernstein, *Phys. Rev.* **187**, 345 (1969).
- ²⁷ E. Akkermans, A. Auerbach, J. E. Avron, and B. Shapiro, *Phys. Rev. Lett.* **66**, 76 (1991).
- ²⁸ Y. Meir and N. S. Wingreen, *Phys. Rev. Lett.* **68**, 2512 (1992).
- ²⁹ V. Gasparian, T. Christen, and M. Büttiker, *Phys. Rev. A* **54**, 4022 (1996).
- ³⁰ C. A. Stafford, D. Baeriswyl, J. Bürki, H. Grabert, and F. Kassubek (unpublished).
- ³¹ A. Szafer and A. D. Stone, *Phys. Rev. Lett.* **62**, 300 (1989).
- ³² A. Weisshaar, J. Lary, S. M. Goodnick, and V. K. Tripathi, *J. Appl. Phys.* **70**, 355 (1991).
- ³³ We wish to thank J. Bürki for useful comments on this point.
- ³⁴ H. Weyl, *Math. Ann.* **71**, 441 (1912).
- ³⁵ M. Kac, *Am. Math. Monthly* **73**, 1 (1966); for a recent discussion, see G. Gutiérrez and J. M. Yáñez, *Am. J. Phys.* **65**, 739 (1997).
- ³⁶ H. P. McKean and I. M. Singer, *J. Diff. Geom.* **1**, 43 (1967).
- ³⁷ S. Ulreich and W. Zwerger, *Europhys. Lett.* **41**, 117 (1998).
- ³⁸ M. F. Crommie, C. P. Lutz, and D. M. Eigler, *Nature* **363**, 524 (1993).
- ³⁹ E. Scheer, N. Agraït, J. C. Cuevas, A. Levy Yeyati, B. Ludoph, A. Martín-Rodero, G. Rubio Bollinger, J. M. van Ruitenbeek, and C. Urbina, *Nature* **394**, 154 (1998).
- ⁴⁰ M. Brandbyge, M. R. Sørensen, and K. W. Jacobsen, *Phys. Rev. B* **56**, 14956 (1997).

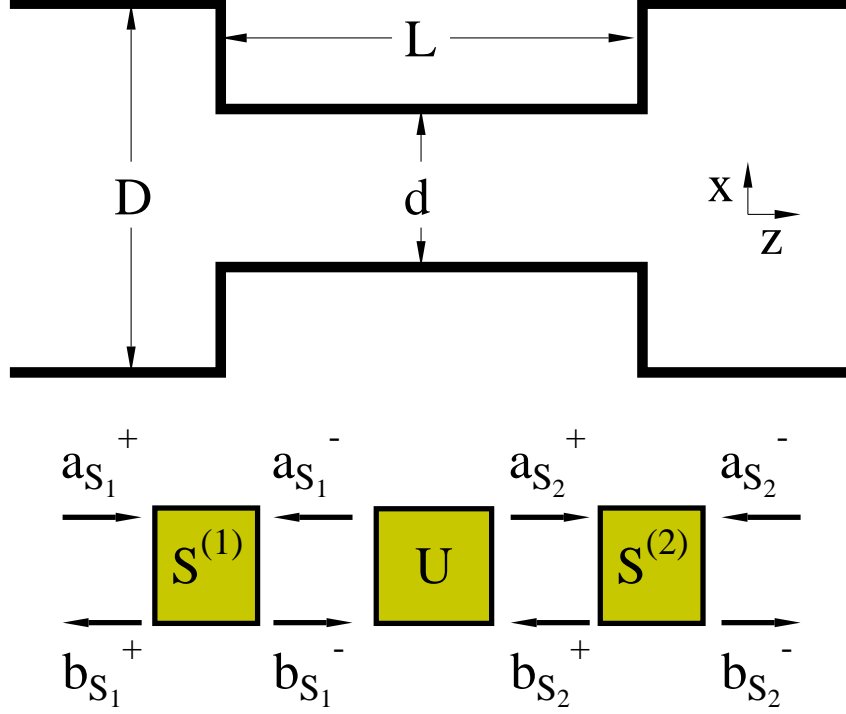


FIG. 1. Schematic diagram of the WNW-Geometry. In the upper part, the wire geometry is sketched. D and d are the diameters of the wide and narrow parts of the wire, respectively. Under elongation, it is assumed that the area of the narrow part of the wire is conserved, $Ld = L_0D = A$, where L_0 is the initial length. In the 3D case, the wire is assumed to have a square cross-section, and the volume of the narrow part is held constant during elongation, $Ld^2 = L_0D^2 = V$. The lower part of the figure shows the scattering scheme: scattering matrices ($S^{(1)}$ and $S^{(2)}$ at WN-transitions and U for the narrow part of the wire) characterize the transmission and reflection of current amplitudes denoted as arrows in the diagram. The total S-matrix relates the outgoing current amplitudes $b_{S_1}^+$ and $b_{S_2}^-$ to the incoming current amplitudes $a_{S_1}^+$ and $a_{S_2}^-$.

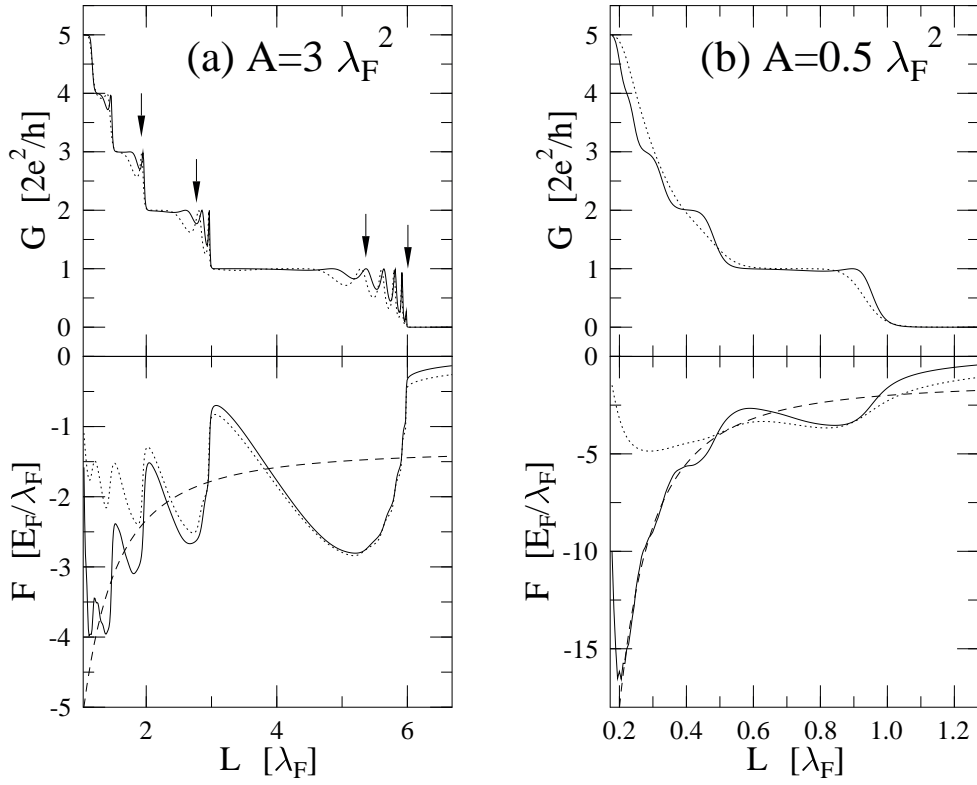


FIG. 2. Electrical conductance and tensile force for two different 2D wires with WNW-geometry as a function of the length L of the narrow part. Assuming area conservation, L is varied from a perfect wire (where narrow and wide parts have the same diameter) until the last conductance channel breaks. (a) A wire with a relatively large area of the narrow part ($A = 3.0\lambda_F^2$) and (b) a wire with a smaller area ($A = 0.5\lambda_F^2$) are shown. The diameter of the wide part is $2.9\lambda_F$, fixing the total number of asymptotically propagating modes to be 5. The dotted curves show the adiabatic approximation to conductance and force, the dashed curves give the surface tension, the leading order contribution in a semiclassical expansion of the force. The arrows indicate the geometries used in Fig. 5.

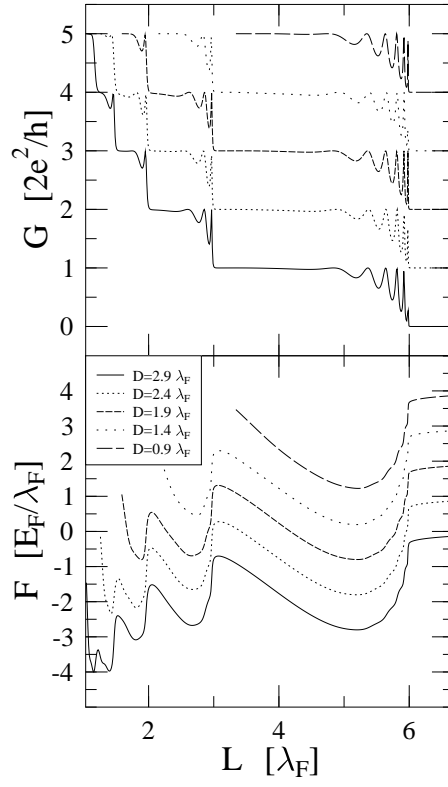


FIG. 3. Electrical conductance and cohesive force for 2D wires with various outer diameters D . The area of the narrow part was held constant, so the initial length (when $D = d$) of the wires is different. The area of the narrow part is $3.0\lambda_F^2$ as in Fig. 2(a). The curves are vertically offset.

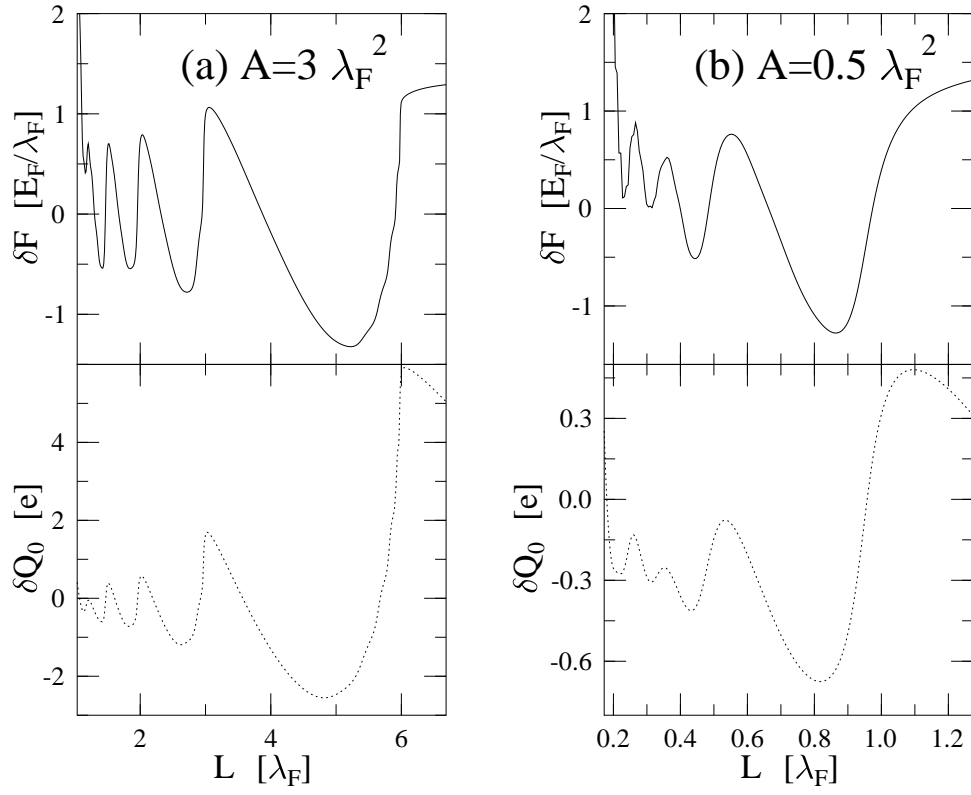


FIG. 4. Force and charge oscillations for two different 2D WNW wires as a function of elongation. Force oscillations are shown in the upper and charge oscillations in the lower half. The wire parameters are the same as in the preceding figures, (a) shows a wire with a larger and (b) a wire with a smaller area of the narrow part.

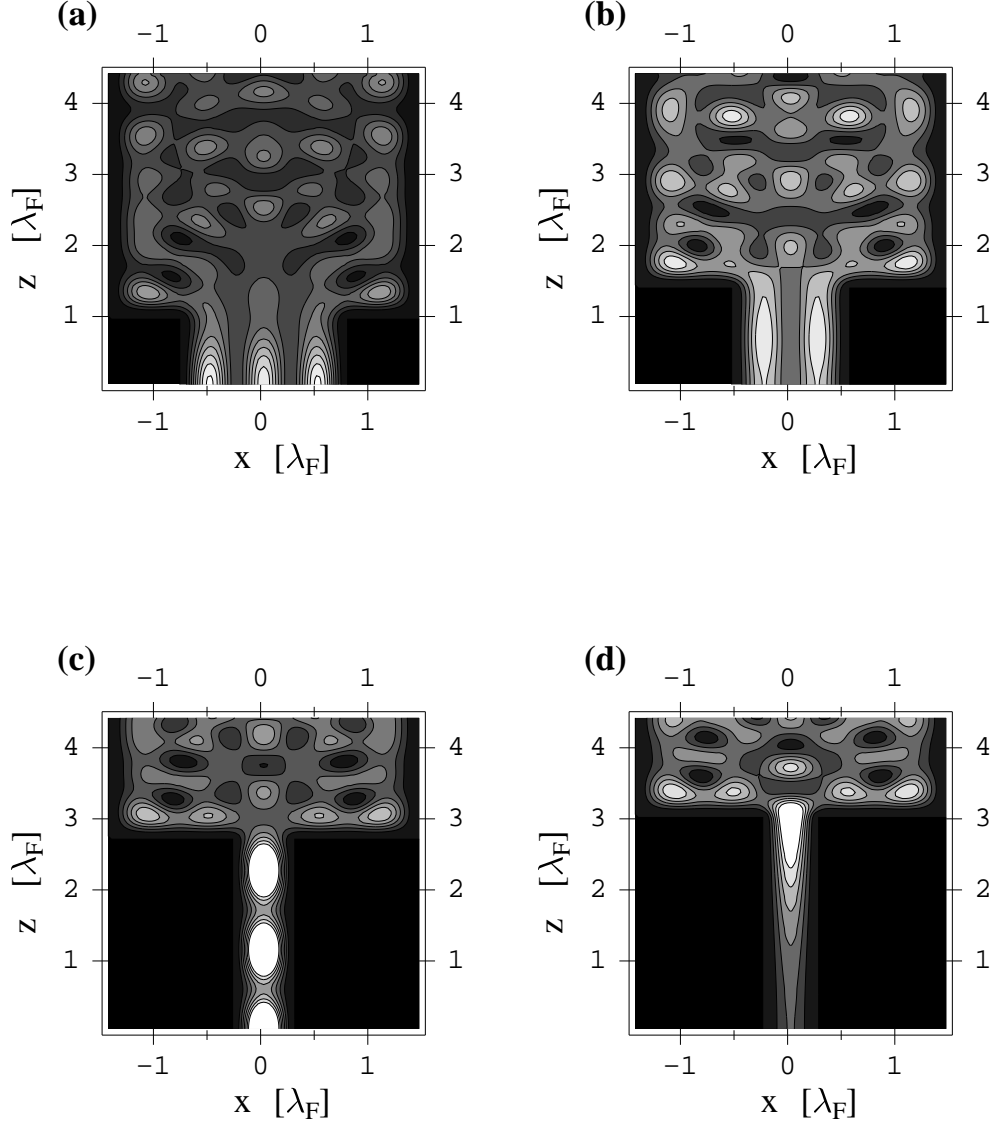


FIG. 5. Local density of states $D(E_F, x, z)$ at the Fermi energy in a 2D wire. The area of the N-part and the diameter of the W-part have been chosen as in Fig. 2(a) ($A = 3.0\lambda_F^2$ and $D = 2.9\lambda_F$) to make comparison with Fig. 2(a) possible. The diameter of the N-part is (a) $2.4\lambda_F$, (b) $1.9\lambda_F$, (c) $1.4\lambda_F$, (d) $0.9\lambda_F$. The corresponding elongations are marked as arrows in the upper part of Fig. 2(a). Black areas correspond to $D = 0.0/(E_F \lambda_F^2)$, white areas to $D > 1.0/(E_F \lambda_F^2)$, contours are drawn at equally spaced values of D between these two limits.

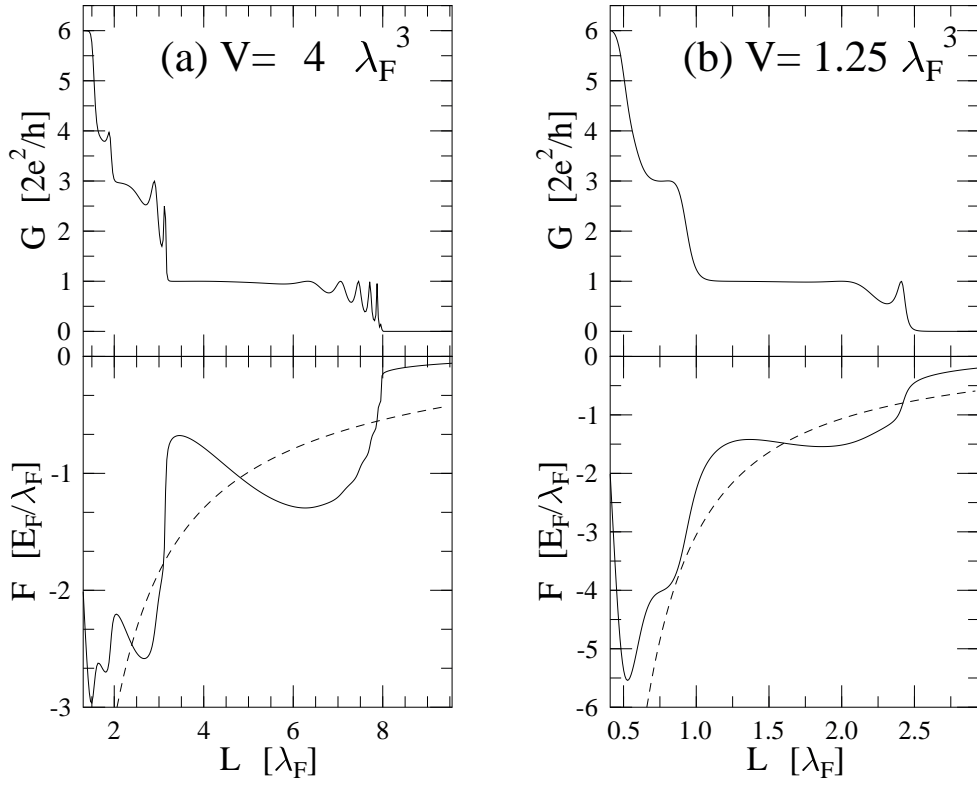


FIG. 6. Electrical conductance and tensile force for two different 3D wires with WNW-geometry and square cross-section as a function of the length L of the narrow part. The width of the narrow part is determined by a constant-volume constraint $Ld^2 = L_0D^2 = V = \text{const}$, where L_0 is the initial length of the constriction before deformation. In (a) the volume of the narrow part is given by $V = 4\lambda_F^3$ while it is smaller ($V = 1.25\lambda_F^3$) in (b). The dimensions in (b) are comparable with those of the Au wire studied experimentally in Ref. 4. The dashed curves give the force expected by the surface term plus topological correction.

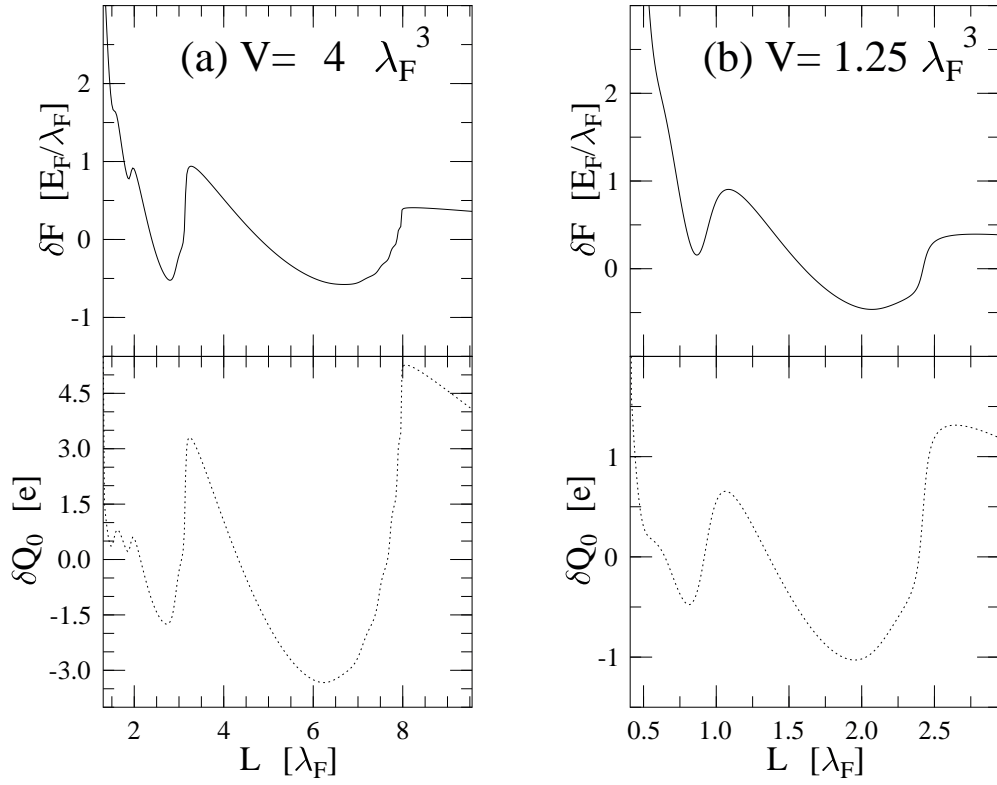


FIG. 7. Charge and force oscillations as a function of elongation for two 3D wires with WNW geometry. The same parameters as in Fig. 6 have been used.

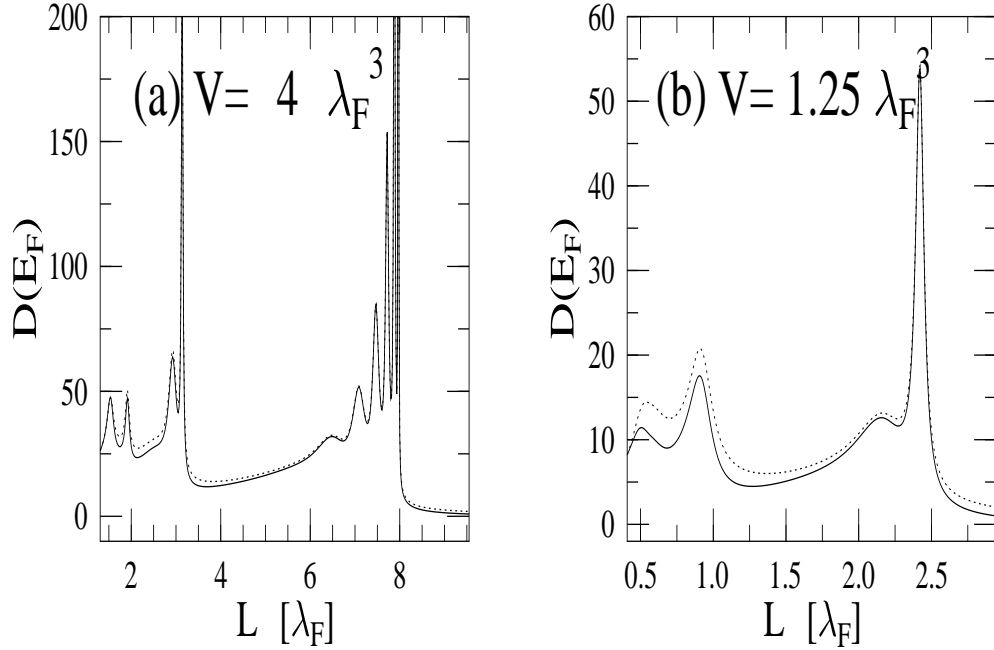


FIG. 8. Density of states at the Fermi surface as a function of elongation for 3D wires with parameters as in Fig. 6. The solid line shows the LDOS integrated over the narrow part of the wire, the dotted line the DOS computed from Eq. (5).